

Towards a standard spin Seebeck measurement

By K. Morrison,^{1*} A.J Caruana,^{1,2} C. Cox¹

[*] Dr K. Morrison

¹Department of Physics, Loughborough University,
Loughborough LE11 3TU (United Kingdom)

²ISIS Neutron and Muon Source, Didcot, Oxfordshire, OX11 0QX

E-mail: k.morrison@lboro.ac.uk

Keywords: Magnetic materials, thermoelectrics, thin films

PACS: 72.25.Mk, 72.25.-b, 75.76.+j

Whilst there have been several reports of the spin Seebeck effect to date, comparison of the absolute voltage(s) measured, in particular for thin films, is limited. In this letter we demonstrate normalization of the spin Seebeck effect for Fe₃O₄:Pt samples deposited on glass with respect to the heat flow, J_q , and temperature difference, ΔT . We show that the choice of substrate can have a significant impact on the measured spin Seebeck voltage irrespective of the sample quality (obtaining $V_{ISHE}/\Delta T L_y = 15\text{-}40 \mu\text{V/K/m}$, or $V_{ISHE} L_z/\Delta T L_y = 0.005\text{-}0.045 \mu\text{V/K}$). Finally, we present a spin Seebeck coefficient for substrate independent characterization of the spin Seebeck effect, where for the Fe₃O₄:Pt bilayers presented here we find $i=1.5\pm 0.1 \mu\text{V/W}$.

The spin Seebeck effect (SSE) is defined as the production of a spin polarized current in a magnetic material subject to a thermal gradient. It was first highlighted by Uchida *et al.* [1], and led to the development of a new field of magnetothermal effects (such as spin Peltier and spin Nernst) now grouped together under spin caloritronics [2].

Observation of the spin Seebeck effect is achieved by placing a heavy metal such as Pt in contact with the magnetic material, where the spin current generated in the magnetic layer is injected into the Pt layer and converted to a useable voltage by the inverse spin Hall effect [3,4]. The advantage of the SSE is that it can be used as a source of pure spin polarized current for spintronics applications that paves the way for a whole host of new devices (such as spin Seebeck based diodes) [5–8]. In addition to its potential applications in spintronics, it has been presented as an alternative to conventional thermoelectrics for harvesting of waste heat, due to decoupling of the electric and thermal conductivities that typically dominate the efficiency [9][10][11]. This is in part due to a completely different device architecture, such as that shown in Figure 1, where the magnetic layer can be chosen to have low thermal conductivity independent of the second paramagnetic layer, which in turn can be selected to have low resistivity.

There are two measurement geometries for the spin Seebeck effect - longitudinal and transverse - as shown in Figure 1(a) & (b). In early work there was some comparison between the two with regards to phonon contributions to the effect and the impact of the anomalous Nernst effect [12]. In this work, however, we discuss the longitudinal SSE (LSSE) only, since this

geometry lends itself readily to energy harvesting. Furthermore, the LSSE is largely absent of artefacts that arise from thermal shunting of the temperature gradient, i.e. where there is a mismatch between the thermal conductivity of the substrate and magnetic thin film [13].

Whilst there have been extensive studies of the spin Seebeck effect over the last 5-10 years, this has predominantly been in the YIG:Pt system, where for thin films, the substrate is often GGG [14][15]. Despite indications of the importance of heat flow in measurements [16], [17], [18], typically longitudinal spin Seebeck measurements are characterized by measuring the voltage generated across two contacts (of a spin convertor layer), as the temperature difference across the substrate, magnetic layer, and Pt is monitored.

If such spin Seebeck devices are to be considered for power conversion - in particular as thin film devices - there needs to be a shift in metrology so that meaningful comparison of the material parameters can be made. This is of particular importance if we consider the impact that the quality of the magnet:Pt interface can have on the observed voltage (i.e. efficiency of spin injection) [14]. An intermediate step is to use a simple thermal model to estimate the temperature difference across the active layer, however, this is limited by the unknown thermal conductivity of the thin films (likely to differ from the bulk) and thermal interface resistances.

Here we present results obtained for various Fe₃O₄:Pt thin films deposited on glass, where both the heat flow, J_Q , and temperature difference, ΔT are monitored. We demonstrate that the substrate can have a significant impact on the measured ‘spin Seebeck’ effect if only ΔT is monitored. We follow this by defining a

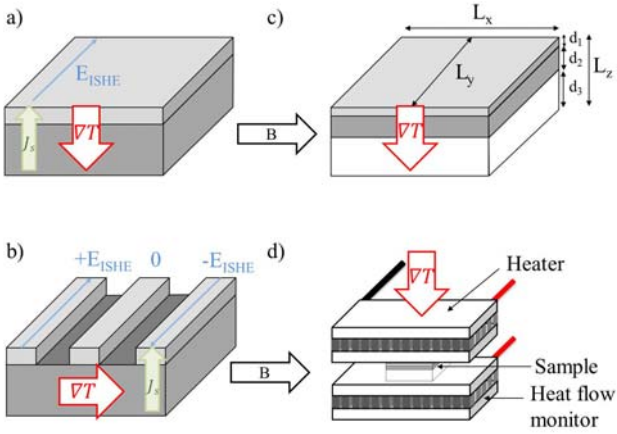


Figure 1 – **a)** & **b)** longitudinal and transverse spin Seebeck measurement geometries. Thermally generated spin current, J_s , is produced in the magnetic layer (dark grey) and converted to a measurable voltage (E_{ISHE}) in the spin convector layer (grey) by the inverse spin Hall effect. **c)** Typical longitudinal spin Seebeck thin film device; the length scales L_x , L_y , and L_z denote device dimensions with respect to the thermal gradient (along z axis). Individual thicknesses of each layer $\{d_1, d_2, d_3\}$ are also indicated. **d)** Schematic of the experimental set-up used in this work.

dimensionless spin Seebeck coefficient that is dependent on J_Q rather than ΔT , and demonstrate that this provides the first step towards a standardized measurement.

The samples tested here were part of a series of 80:5 nm thick Fe_3O_4 :Pt bilayers deposited using pulsed laser deposition (PLD) in ultra-high vacuum (base pressure 5×10^{-9} mbar) onto 0.15 mm, 0.3 mm and 0.5 mm thick borosilicate glass and 0.6 mm or 0.9 mm fused silica substrates. The laser fluence and substrate temperature for Fe_3O_4 and Pt deposition were 1.9 ± 0.1 J/cm² and 3.7 ± 0.2 J/cm², and 400 C and 25 C, respectively. Fe_3O_4 was chosen due to its large spin polarization ($\sim 80\%$ [19]), low thermal conductivity (at 300 K: $\kappa_{thin\ film} \sim 2-3.5$ W m⁻¹ K⁻¹, [20] $\kappa_{bulk} \sim 2-7$ W m⁻¹ K⁻¹ [21]), and relative abundance of the constituent elements. Of particular note are the following: X-ray reflectivity data indicated a typical Pt thickness across the series of 4.5 ± 0.5 nm and a roughness $\sigma = 1.5 \pm 0.2$ nm. Fe_3O_4 thickness was varied from 20 to 320 nm. Further details are given in [18] and the supplementary information.

Magnetic characterization was obtained using a Quantum Design Magnetic Property Measurement System (SQUID) as a function of temperature and field. Room temperature coercive loops were confirmed for each sample using a Magneto-Optic Kerr effect (MOKE) magnetometer. Magnetometry at room temperature typically exhibited a coercive field, $H_c = 197 \pm 5$ Oe, saturation magnetization, $M_s = 90$ A m² kg⁻¹, and a remanent moment of $M_r = 68$ A m² kg⁻¹.

Spin Seebeck measurements were obtained from a set-up similar to that of Sola *et al.* [16] The thin film

was sandwiched between 2 Peltier cells, where the top Peltier cell (1) acted as a heat source, and the bottom Peltier cell (2) monitored the heat current, J_Q , through the sample. The Peltier cells were calibrated by monitoring the Peltier voltage, V_P , generated as a current was passed through surface mount resistors fixed to the top side of the Peltier cell (where the sensitivity, S_p was found to be 0.11 V/W at 300K). Two type E thermocouples mounted on the surface of the Peltier cells (such that they are in contact with the sample during the measurement) monitored the temperature difference across the sample, ΔT ; a schematic of this set-up is given in Figure 1(d).

It is useful at this point to note some key characteristics of the SSE: First, the voltage has been shown (for a single device) to increase linearly with temperature difference (ΔT) [9] or heat flow (J_Q) [16]. Secondly, it is known to increase linearly with contact separation (L_y) [9]. Lastly, for thin films, there have been indications of a length scale of the order of the magnon free path length above which the voltage generated saturates [22] [23].

In response to these observations, some of the first attempts to quantify the SSE were to normalize the voltage measured, V_{ISHE} , to the temperature difference, ΔT ,

$$S_1 = \frac{V_{ISHE}}{\Delta T} \quad (1)$$

where the units are ($\mu\text{V}/\text{K}$). More accurately, this could also be normalized to contact separation, L_y

$$S_2 = \frac{V_{ISHE}}{L_y \Delta T} \quad (2)$$

with units of ($\mu\text{V}/\text{K}/\text{m}$).

Given that the spin Seebeck effect is defined in terms of the thermal gradient across the magnetic material, ∇T , for bulk samples, the spin Seebeck coefficient is more often defined as

$$S_3 = -\frac{E_{ISHE}}{\nabla T} = \frac{V_{ISHE} L_z}{L_y \Delta T} \quad (3)$$

where the units are ($\mu\text{V}/\text{K}$), and the thermal gradient ∇T can be described by the temperature difference, ΔT , divided by the thickness of the sample, L_z .

It was shown recently by Sola *et al.*, that for thin film samples in particular there is the added complication of thermal resistance between the sample and the hot and cold baths (i.e. the interface across which ΔT is measured) [17]. Here they showed in measurements of the same sample in an experimental set-up at both INRIM and Bielefeld that the measurement as a function of ΔT was unreliable – differing by a factor of 4.6 (gave $S_3 = 0.231$ $\mu\text{V}/\text{K}$ and

0.0496 $\mu\text{V}/\text{K}$, respectively), whereas by normalizing to heat flow, both set-ups obtained the same value to within 4% ($S_3 = 0.685$ and $0.662 \mu\text{V}/\text{K}$, respectively).

In this work they measured the heat flow, J_Q , using a calibrated Peltier cell and initially determined the normalized voltage generated per unit of heat flow

$$S_4 = \frac{V_{ISHE}}{L_y \left(\frac{Q}{A_T} \right)} \quad (4)$$

where Q is the heat passing through a sample with cross-sectional area surface, A_T , and the units are ($\mu\text{V}\cdot\text{m}/\text{W}$). Given that the thermal conductivity can be defined by

$$\kappa = \left(\frac{Q}{A_T} \right) / \left(\frac{\Delta T}{L_z} \right) \quad (5)$$

where $J_Q = Q/A_T$, they argued that S_3 (equation 3) could be estimated by multiplying S_4 (equation 4) by κ . This was based on using a simple linear model that assumed that the thermal conductivity of the substrate and magnetic film were well matched.

For samples where the thermal conductivity is not well matched, we showed previously that the substrate plays a significant role in determining the value of ΔT across the active material – the magnetic layer – in a thin film device [2]. This highlights a significant disadvantage of using the spin Seebeck coefficients, outlined in equations (1)-(3) for thin film devices. To circumvent this problem, we argue that in the equilibrium condition a simple thermal model can be used to determine the heat flow through the entire sample

$$Q = \frac{A_T \Delta T}{d_1/\kappa_1 + d_2/\kappa_2 + d_3/\kappa_3} \quad (6)$$

where $\{d_1, d_2, d_3\}$ and $\{\kappa_1, \kappa_2, \kappa_3\}$ are the thicknesses and thermal conductivities of the top layer (1), FM layer (2) and substrate (3), respectively; ΔT is the temperature difference across the entire device. It can be seen from this, that the temperature gradient is a function of the thermal conductivities of each layer and that the temperature difference across the ‘active’ magnetic layer can be thermally shunted by substrates with relatively low thermal conductivities (for example, see the comparison made between SrTiO_3 and glass $\text{Fe}_3\text{O}_4:\text{Pt}$ in [18]).

Of course, this is an oversimplification as it does not take into account any temperature drops at interfaces. Given that J_Q will be constant across the sample once thermal equilibrium has been reached, and that it will be proportional to the temperature gradient across the active magnetic layer, of thickness d_2 , we can write the thermal gradient as

$$\nabla T' = \frac{\Delta T'}{d_2} = \frac{J_Q}{d_2} \left(\frac{d_2}{\kappa_2} \right) = \frac{J_Q}{\kappa_2} \quad (7)$$

where for the magnetic layer $L_z = d_2$ and we now have a direct relationship between the thermal gradient and the heat flow, J_Q . Therefore, it should be reasonable to define a spin Seebeck coefficient that is not reliant on knowledge of the thermal conductivity of the sample and substrate (equation (4)).

To test this, we prepared several $\text{Fe}_3\text{O}_4:\text{Pt}$ samples on glass substrates of varying thickness, where the Pt thickness was kept at 5 nm (± 0.5 nm) in order to minimize any variation due to Pt thickness [18]. The spin Seebeck voltage was then measured for various thermal gradients as a function of applied magnetic field.

We found that for the same sample, the aspect ratio and total contact area could have an impact on the determination of S_4 . This was tested by taking one of the $\text{Fe}_3\text{O}_4:\text{Pt}$ samples from our study (22x22x0.5 mm glass substrate, 80 nm Fe_3O_4 , 5 nm Pt) and measuring in various orientations. First, a buffer layer between the

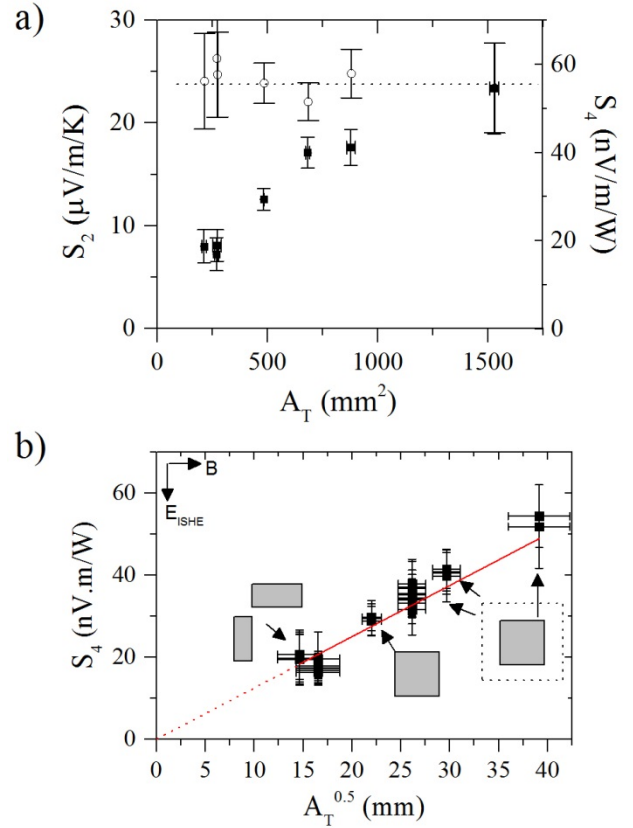


Figure 2 – Summary of normalization measurements. (a) S_2 and S_4 as a function of A_T (as L_z is fixed S_2 and S_3 are equivalent). (c) S_4 as a function of $A_T^{0.5}$. Inset sketches indicate aspect ratio for the individual data points. The dotted line indicates measurements where a buffer layer (same thickness glass substrate) was inserted in order to increase A_T . Errors were determined from the combination of uncertainty in contact separation, L_y , thermal contact area, A_T , and the noise floor of the V_{ISHE} voltage.

two Peltier cells was introduced (same thickness as the substrate – on the assumption that control of J_Q by the magnetic layer is largely negligible). This effectively increased the thermal contact area, A_T , whilst L_y and L_z were fixed. Secondly, the 22x22 mm sample was cleaved in two and measured along the long and short sides, thus changing A_T , the aspect ratio and L_y .

The spin Seebeck coefficients S_2 , S_3 , S_4 (equations 2-4) were then calculated, as shown in Figure 2. S_2 and S_3 were constant (within error) for all data on this sample, which is not unexpected as aside from changes in sample dimensions, the spin Seebeck effect should remain unchanged. As S_3 normalizes for the thickness L_z , which is constant in this measurement it is expected to be directly proportional to S_2 .

Upon normalizing to heat flow, however, as shown in Figure 2(b), the spin Seebeck coefficient we obtained (S_4) was no longer constant. Given that we do not expect the spin Seebeck effect to have changed for this sample, we plotted this data as a function of various parameters – e.g. L_x , L_y , L_y/L_x , A_T/L_y , A_T and finally $A_T^{0.5}$ (see the supplementary information). The only way we have found so far to reduce S_4 into a constant for our known sample (i.e. a linear relationship with respect to S_4), was to divide through by $A_T^{0.5}$, as shown in Figure 2

(c). This in itself is interesting for two reasons: (1) the coefficient we now obtain is independent of geometry (units of $\mu\text{V}/\text{W}$); and (2) it suggests that the relationship between S_3 and S_4 is not as straightforward as expected. One possible reason for this could be the need to reduce the data from a two dimensional measurement of the heat flux (normalized per unit area), to a voltage measured along one dimension (L_y). For example, for a simple geometry where $A_T = L_x L_y$

$$S_5 = \frac{S_4}{A_T^{0.5}} = \frac{V_{ISHE} A_T}{L_y Q A_T^{0.5}} = \frac{V_{ISHE} L_x^{0.5}}{Q L_y^{0.5}} \quad (8)$$

and this definition of the spin Seebeck coefficient is now normalized by the total heat through the sample *and* the square root of the aspect ratio (L_y/L_x).

As stated earlier, the advantage of defining a spin Seebeck coefficient dependent on J_Q rather than ΔT is that it will be independent of thermal contact resistance [16], and the substrate. In Figure 3 we show the results of spin Seebeck measurements for our Fe_3O_4 :Pt bilayers as a function of substrate and Fe_3O_4 thickness ($t_{\text{substrate}}$ and $t_{\text{Fe}_3\text{O}_4}$ respectively). Note that there was a scatter in our individual data points that can be attributed to varying thermal resistance between each

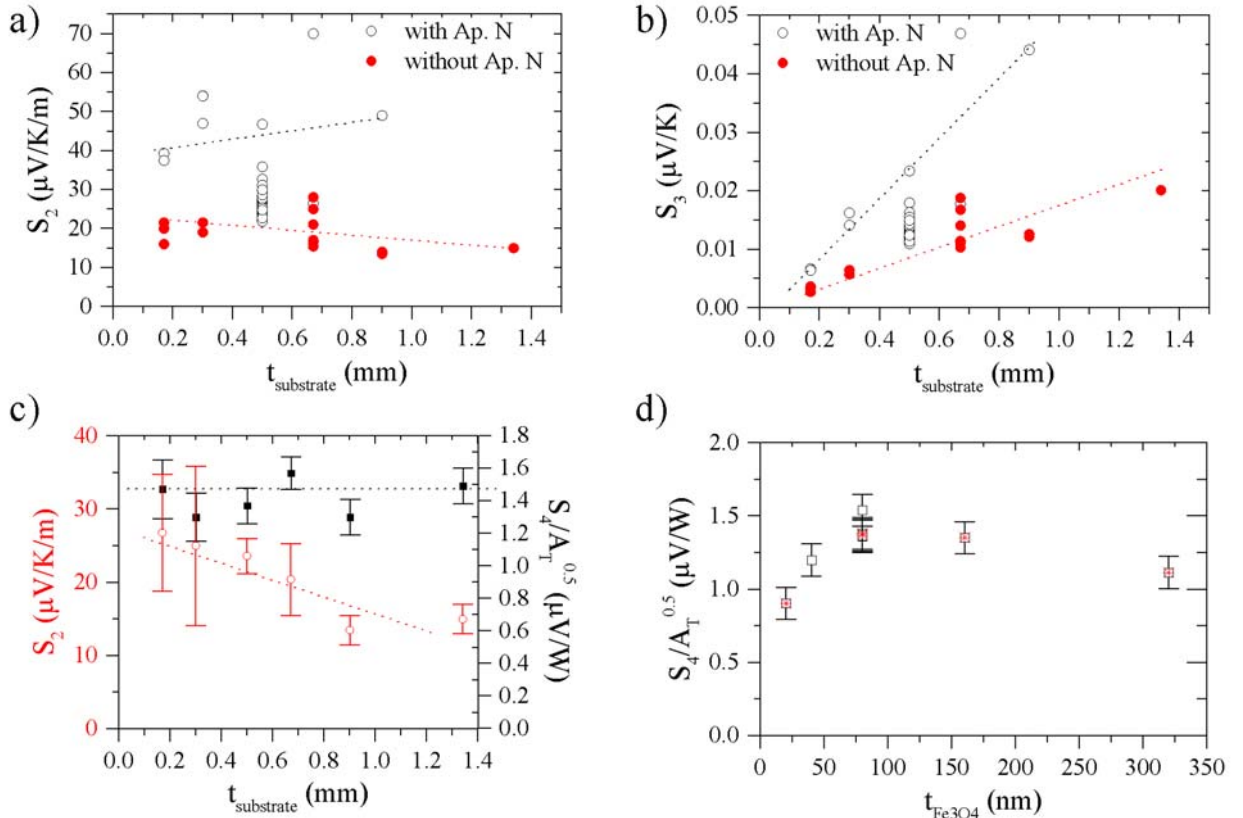


Figure 3 – Summary of spin Seebeck measurements as a function of substrate and Fe_3O_4 thickness, $t_{\text{substrate}}$ and $t_{\text{Fe}_3\text{O}_4}$, respectively (a) S_2 and (b) S_3 as a function of $t_{\text{substrate}}$. The scatter in data points indicates a change in thermal contact resistance for samples measured multiple times (with sample mounting/unmounting in between). Open/closed symbols indicate measurements with/without Apiezon NTM thermal grease to aid thermal contact. Lines are guides for the eye. (c) Average value for S_2 and $S_4/A_T^{0.5}$ as a function of the $t_{\text{substrate}}$. (d) $S_4/A_T^{0.5}$ as a function of $t_{\text{Fe}_3\text{O}_4}$.

measurement for the same samples measurements were taken several times. To demonstrate this we show measurements with and without Apiezon NTM thermal grease, where in both cases the sample was clamped between the hot and cold sinks (in our case the Peltier cell surfaces). The thermal grease would be expected to improve the thermal contact at the sample:Peltier interface, thus decreasing any temperature drop at the sample:Peltier interface. In Figure 3 (c) we show a summary of all measurements as a function of thickness. As can be seen, S_2 decreased linearly with increasing thickness, as a larger proportion of ΔT is shunted across the substrate. As soon as the data was normalized for J_Q ($S_4/A_T^{0.5}$), as is also shown in Figure 3(c) we obtained a relatively constant value (within error, and any variation that might be expected is due to interface quality [14] or small differences in t_{Pt} and the resistance), compared to irregular data for calculation of S_3 and S_2 shown in Figure 3(a)-(c). With regards to the thickness dependence of the spin Seebeck effect (Figure 3(d)) we also see collapse of the data onto the expected saturation at around 80 nm.

REFERENCES

[1] K. Uchida, S. Takahashi, K. Harii, J. Ieda, W. Koshihara, K. Ando, S. Maekawa, and E. Saitoh, *Nature* **455**, 778 (2008).

[2] G. E. W. Bauer, E. Saitoh, and B. J. van Wees, *Nat. Mater.* **11**, 391 (2012).

[3] T. Jungwirth, J. Wunderlich, and K. Olejnik, *Nat. Mater.* **11**, 382 (2012).

[4] A. Hoffmann, *IEEE Trans. Magn.* **49**, 5172 (2013).

[5] S. Borlenghi, W. Wang, H. Fangohr, L. Bergqvist, and A. Delin, *Phys. Rev. Lett.* **112**, 1 (2014).

[6] H.-H. Fu, D.-D. Wu, L. Gu, M. Wu, and R. Wu, *Phys. Rev. B* **92**, 45418 (2015).

[7] J. Ren, J. Fransson, and J. X. Zhu, *Phys. Rev. B - Condens. Matter Mater. Phys.* **89**, 1 (2014).

[8] L. Gu, H. H. Fu, and R. Wu, *Phys. Rev. B - Condens. Matter Mater. Phys.* **94**, 1 (2016).

[9] K. Uchida, M. Ishida, T. Kikkawa, a Kirihara, T. Murakami, and E. Saitoh, *J. Phys. Condens. Matter* **26**, 343202 (2014).

[10] S. R. Boona, S. J. Watzman, and J. P. Heremans, *APL Mater.* **4**, (2016).

[11] K. I. Uchida, H. Adachi, T. Kikkawa, A. Kirihara, M. Ishida, S. Yorozu, S. Maekawa, and E. Saitoh, *Proc. IEEE* **104**, 1946 (2016).

[12] M. Schmid, S. Srichandan, D. Meier, T. Kuschel, J.-M. Schmalhorst, M. Vogel, G. Reiss, C. Strunk, and C. H. Back, *Phys. Rev. Lett.* **111**, 187201 (2013).

To summarize, we have demonstrated that the heat flow method is suitable for obtaining substrate independent measurements of the spin Seebeck effect, where the thermal conductivity of the thin film need not be known, and have proposed an alternative spin Seebeck coefficient for comparison of different material systems. By measuring the spin Seebeck effect as the thickness of the substrate, Fe₃O₄ layer and sample dimensions $\{L_x, L_y, A_T\}$ were varied, we demonstrated that for the same material system (assuming t_{Pt} is constant) that this method reliably returned a value of $1.5 \pm 0.1 \mu\text{V}/\text{W}$. Since this result holds for different values of $t_{substrate}$, the heat flow normalization method could, therefore, be used to compare similar samples where the substrate thickness or type were varied.

ACKNOWLEDGEMENTS

This work was supported by EPSRC First Grant (EP/L024918/1) and Fellowship (EP/P006221/1) and the Loughborough School of Science Strategic Major Operational Fund. KM would also like to thank M.D. Cropper for their help with use of the PLD system for sample fabrication.

[13] S. Y. Huang, W. G. Wang, S. F. Lee, J. Kwo, and C. L. Chien, *Phys. Rev. Lett.* **107**, 216604 (2011).

[14] Z. Qiu, D. Hou, K. Uchida, and E. Saitoh, *J. Phys. D. Appl. Phys.* **48**, 164013 (2015).

[15] T. Kikkawa, K. Shen, B. Flebus, R. A. Duine, K. I. Uchida, Z. Qiu, G. E. W. Bauer, and E. Saitoh, *Phys. Rev. Lett.* **117**, 1 (2016).

[16] A. Sola, M. Kuepferling, V. Basso, M. Pasquale, T. Kikkawa, K. Uchida, and E. Saitoh, *J. Appl. Phys.* **117**, 17C510 (2015).

[17] A. Sola, P. Bougiatioti, M. Kuepferling, D. Meier, G. Reiss, M. Pasquale, T. Kuschel, and V. Basso, *Nat. Publ. Gr.* **1** (2017).

[18] A. J. Caruana, M. D. Cropper, J. Zipfel, Z. Zhou, G. D. West, and K. Morrison, *Phys. Status Solidi - Rapid Res. Lett.* **10**, 613 (2016).

[19] Y. S. Dedkov, U. Rüdiger, and G. Güntherodt, *Phys. Rev. B* **65**, 64417 (2002).

[20] N.-W. Park, W.-Y. Lee, J.-A. Kim, K. Song, H. Lim, W.-D. Kim, S.-G. Yoon, and S.-K. Lee, *Nanoscale Res. Lett.* **9**, 96(8pp) (2014).

[21] G. a Slack, *Phys. Rev.* **126**, 427 (1962).

[22] A. Kehlberger, U. Ritzmann, D. Hinzke, E.-J. Guo, J. Cramer, G. Jakob, M. C. Onbasli, D. H. Kim, C. a. Ross, M. B. Jungfleisch, B. Hillebrands, U. Nowak, and M. Kläui, *Phys. Rev. Lett.* **115**, 96602 (2015).

[23] A. Anadon, R. Ramos, I. Lucas, P. A. Algarabel, L. Morellon, M. R. Ibarra, and M. H. Aguirre, *Appl. Phys. Lett.* **109**, 12404 (2016).

Supplementary information for “Towards a standard spin Seebeck measurement”

K. Morrison¹, A J Caruana^{1,2}, C. Cox¹

¹ Department of Physics, Loughborough University, Loughborough, LE11 3TU, United Kingdom

² ISIS Neutron and Muon Source, Didcot, Oxfordshire, OX11 0QX

Received ZZZ, revised ZZZ, accepted ZZZ

Published online ZZZ (Dates will be provided by the publisher.)

Keywords Magnetic materials, thermoelectrics, thin films

1 Introduction Extensive experimental details and additional characterization of the films presented in “Towards a standard spin Seebeck measurement” is given in this supporting information.

Additional X-ray diffraction (XRD), resistivity and X-ray reflectivity (XRR) data is used to demonstrate the quality of Fe₃O₄ deposition – exhibiting the characteristic Verwey transition for this phase[1], as well as the expected magnetic characteristics as a function of temperature. This is followed by additional XRD, and XRR data for the Fe₃O₄:Pt bilayers to further demonstrate the magnetic and structural quality of the films.

Finally, example spin Seebeck measurements are given, alongside the additional plots of the spin Seebeck voltage normalized to heat flux, J_Q , as discussed in the main text.

2 Experimental Details

2.1 Sample preparation The series of films prepared for this study are listed in Table S1. They were prepared in vacuum (base pressure of 5×10^{-9} mbar) by pulsed laser deposition (PLD) using a frequency doubled Nd:YAG laser (Quanta Ray GCR-5) with a wavelength of 532 nm and 10 Hz repetition rate. The films were deposited onto 10 x 10 mm and 22 x 22 mm glass slides (Agar Scientific borosilicate coverglasses), or 24 x 32 and 50 x 50 mm fused silica, which were baked out at 400 °C prior to the growth of the Fe₃O₄ layer at the same substrate temperature. The samples were then left to cool in vacuum until they reached room temperature, at which point the Pt layer was deposited. The Fe₃O₄ and Pt layers were deposited from stoichiometric Fe₂O₃ (Pi-Kem purity 99.9%) and elemental Pt (Testbourne purity 99.99%) targets using ablation fluences of 1.90.1 and 3.70.2 J/cm² respectively. The target to substrate distance was 110 mm. The Pt layer thickness was kept constant at 5 ± 0.5 nm for all films, whilst the substrate and Fe₃O₄ thicknesses were varied.

2.2 Structural characterization XRD data was obtained using a Bruker D2 Phaser in the standard Bragg-Brentano geometry using Cu K_α radiation; a Ni filter was used to remove the Cu K_β line. The samples were rotated at a constant 15 rpm throughout the scan to increase the number of crystallites being sampled. XRR measurements

were undertaken using a modified Siemens D5000 diffractometer comprising a graphite monochromator reflecting only Cu K_α into the detector. The incident beam was collimated with a 0.05 mm divergence slit, while the reflected beam was passed through a 0.2 mm anti-scatter slit followed by a 0.1 mm resolution slit. XRR data was fitted using the GenX software package [2].

2.2 Magnetic and electric characterization

Magnetization as a function of applied magnetic field was measured using a Quantum Design Magnetic Properties Measurement System (SQUID). Several bilayer samples were characterized as a function of field at room temperature, whilst the Fe₃O₄ film (without Pt contact) was measured at 5 K, 100-130 K, and 295 K in order to observe the characteristic magnetic Verwey transition at 115 K.

Room temperature sheet resistance was obtained using the Van der Pauw method with a Keithley 6221/2182 nanovoltmeter and current source in conjunction with a Keithley 705 scanner.

Spin Seebeck measurements were obtained from a set-up similar to that of Sola *et al.* [3] The thin film was sandwiched between 2 Peltier cells, where the top Peltier cell (1) acted as a heat source, and the bottom Peltier cell (2) monitored the heat current, J_Q , through the sample. The Peltier cells were calibrated by monitoring the Peltier voltage, V_p , generated as a current was passed through surface mount resistors fixed to the top side of the Peltier cell (where the sensitivity, S_p was found to be 0.11 V/W at 300K). Two type E thermocouples mounted on the surface of the Peltier cells (such that they are in contact with the sample during the measurement) monitored the temperature difference across the sample, ΔT .

3 Results

3.1 Characterization of the Fe₃O₄ layer

Additional characterization data for the Fe₃O₄ thin films (deposited under identical conditions as the devices measured, but without the Pt top layer) is given in Fig. S1.

The Verwey transition is a characteristic feature of the Fe₃O₄ phase of iron oxide and manifests as a sharp increase in resistivity and hysteresis below the Verwey transition temperature (typically between 115 and 120 K)[1]. This feature is clearly seen in Fig. S1 (a), where magnetometry shows a sudden increase in hysteresis below 120 K.

In addition, XRD indicates a preference for <111> texture that is moderately sensitive to the direction of the plume during PLD (see repeated film depositions of Fig. S1 (c)). Due to the instability of the Fe₃O₄ phase, some Fe is also present.

Finally, an example of the X-ray Reflectivity (XRR) fits used to obtain film thickness is given in Figure S1 (d).

3.2 Characterization of the Fe₃O₄:Pt bilayers

Additional characterization data for the Fe₃O₄:Pt bilayers is given in Fig. S2 and S3. Previous work showed that for $t_{Pt} > 2$ nm a thin continuous paramagnetic Pt layer deposited on top of the Fe₃O₄ layer follows the wavy surface of the Fe₃O₄ layer. The Pt stacks on top of the Fe₃O₄ (111) planes and the two grains have an orientation relationship of [011]Pt//[011]Fe₃O₄, (111)Pt//(111)Fe₃O₄, which minimizes the interface energy due to minimal lattice mismatch of $d(111)_{Pt}$ (0.226 nm; JCPDS card 4-802) and $d(222)_{Fe_3O_4}$ (0.242 nm; JCPDS card 19-629).

XRD and XRR data for the sample series where the substrate thickness was varied is given in Fig. S2. Notice that the XRR indicates similar Pt thickness (low frequency ‘bumps’ in the data) as well as some variation in the interface quality (whether high frequency fringes can be observed indicates the relative roughness of the substrate, Fe₃O₄ and Pt layers).

Fig. S3 shows the XRD and magnetization measurements of the sample series where the Fe₃O₄ thickness was varied. Of particular note is the saturation

of the magnetic moment of Fe₃O₄ measured at 1 T for thicknesses > 80 nm.

3.3 Additional spin Seebeck data

Fig. S4 shows a typical spin Seebeck measurement as a function of applied magnetic field. Notice that the corresponding SQUID magnetometry maps exactly to the observed spin Seebeck voltage. The linearity of the measured heat flow with respect to the temperature difference, ΔT , is also shown.

Fig. S5 shows the spin Seebeck voltage normalized by heat flow – $S_4 = V_{ISHE} A_T / Q L_y$ – as a function of the sample parameters L_x , L_y , L_z , L_y/L_x , A_T/L_y , A_T and $A_T^{0.5}$. These measurements were all taken from the same sample as the sample geometry (A_T , L_x and L_y) was varied. As discussed in the main text, a linear trend was only observed for $S_4(A_T^{0.5})$ – Fig S5(f).

References

- [1] F. Walz, J. Phys. Condens. Mat. **14**, R285-R340 (2002).
- [2] M. Björck, and G. Andersson, J. Appl. Cryst. **40**, 1174-1178 (2007).
- [3] A. Sola, M. Kuepferling, V. Basso, M. Pasquale, T. Kikkawa, K. Uchida, and E. Saitoh, J. Appl. Phys. **117**, 17C510 (2015)

Table S1 Summary of the samples measured. The contact separation and corresponding thermal contact area, A_T , are also indicated. There were 2 distinct series of sample: (a) where the Fe₃O₄ and Pt thicknesses ($t_{Fe_3O_4}$ and t_{Pt}) were kept constant (at a nominal 80 nm:5 nm) and the substrate thickness ($t_{substrate}$) was varied, and (b) where the Fe₃O₄ thickness was varied from 20 – 320 nm, whilst the Pt thickness was kept constant. Actual film thickness(es) were determined from fitting XRR data.

Sample	A_T (mm ²)	L_v (mm)	Substrate	$t_{substrate}$ (mm)	t_{Pt} (nm)	$t_{Fe_3O_4}$ (nm)
FP1	768	28.8	Glass	0.17	~4.8	80
FP3 (G6)	136.8	8.47	Glass	0.3	4.9	80
(FP3 frag)	203	12.4				
FP5 (G34)	484, 684, 880, 1530	19.3 19.3	Glass	0.5	5.5	80
	214	7.62				
	270	19.44				
FP6	772	28.56	Fused silica	0.67	4.8	80
				0.67+0.67		
FP9	983	36.66	Fused silica	0.9	5.4	80
F320P (G27)	66.6	6.58	Glass	0.3	4.4	320
F40P (G30)	100	6.26	Glass	0.3	5.2	40
F160P (G31)	100	5.5	Glass	0.3	4.5	160
F20P (G32)	100	7.25	Glass	0.3	5	20

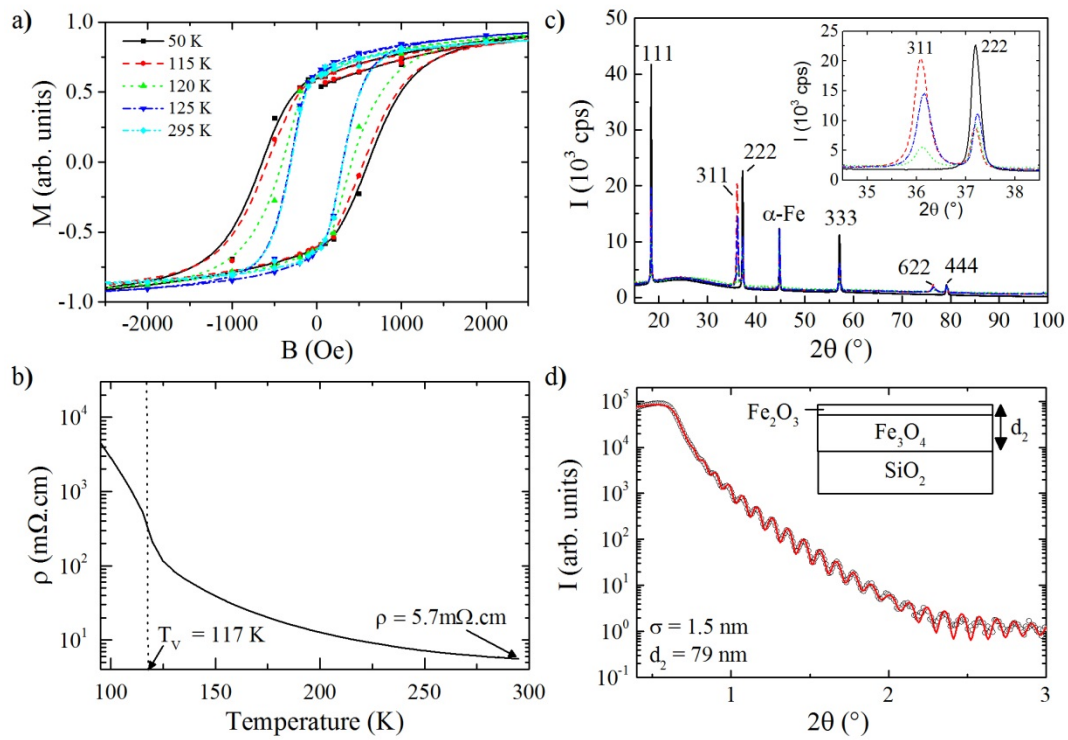


Figure S1 Characterization of the Fe_3O_4 film. a) SQUID magnetometry above and below the Verwey transition, T_V . b) Resistivity as a function of temperature. c) XRD of a set of 4 separately prepared Fe_3O_4 films. The inset shows a close-up of the (311), (222) peaks. d) Example XRR data (symbols) and fit (solid line), indicating thickness = 79 nm, roughness = 1.5 nm.

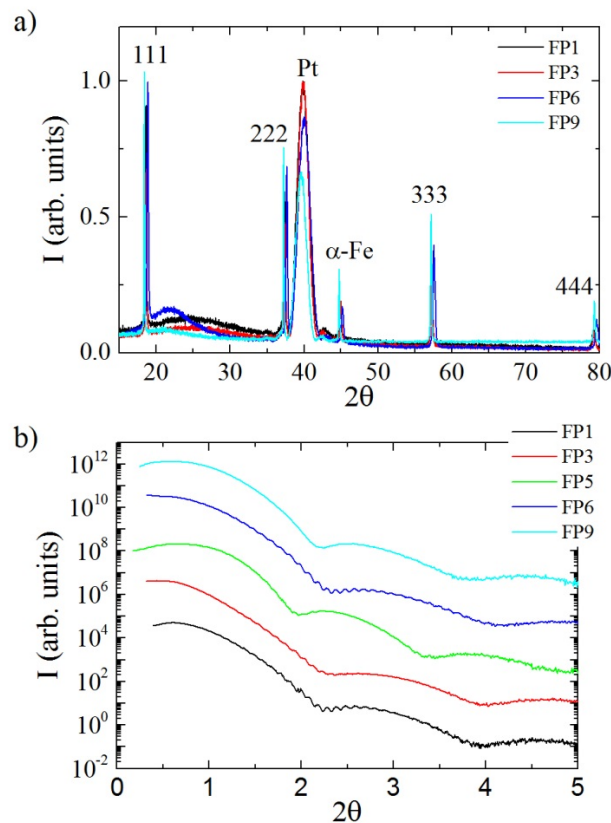


Figure S2 Characteristics of the bilayer film. a) XRD of the Fe_3O_4 :Pt samples where substrate thickness was varied. Note that the amorphous background from the substrate increased with thickness. b) Corresponding XRR data – offset for clarity.

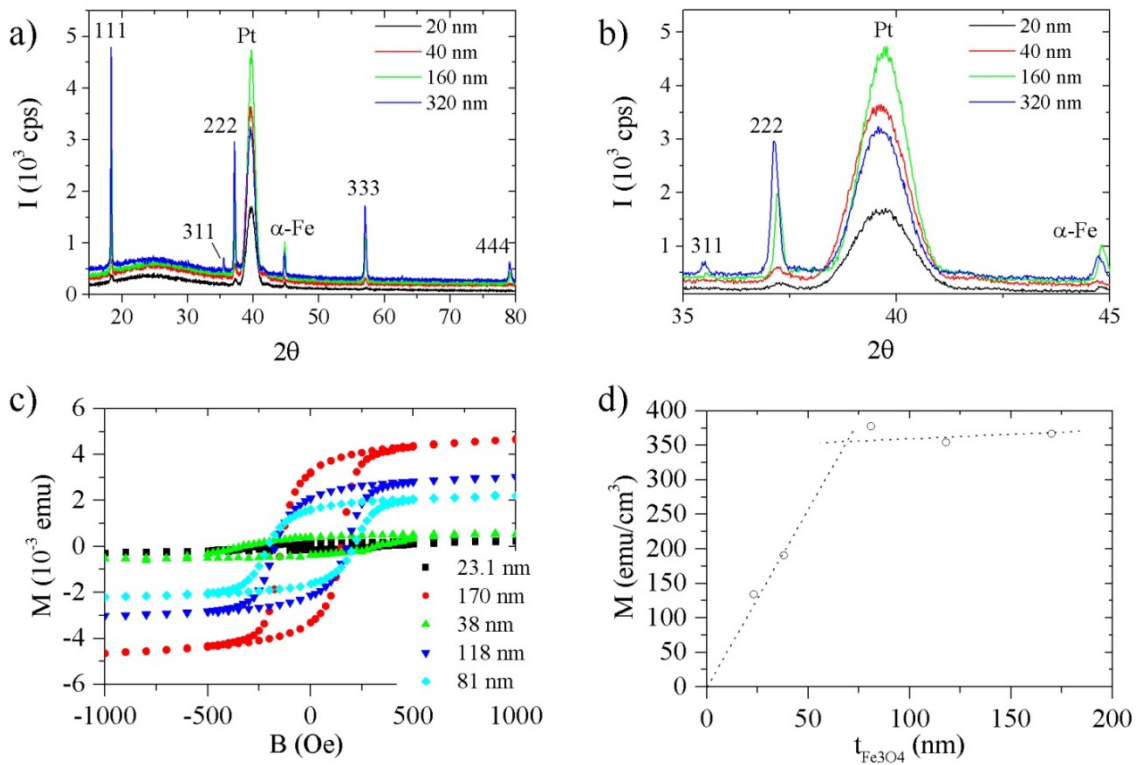


Figure S3 Characteristics of the bilayer films as $t_{Fe_3O_4}$ was varied. a) and b) XRD c) SQUID magnetometry as a function of field, and d) Saturation moment as a function of $t_{Fe_3O_4}$.

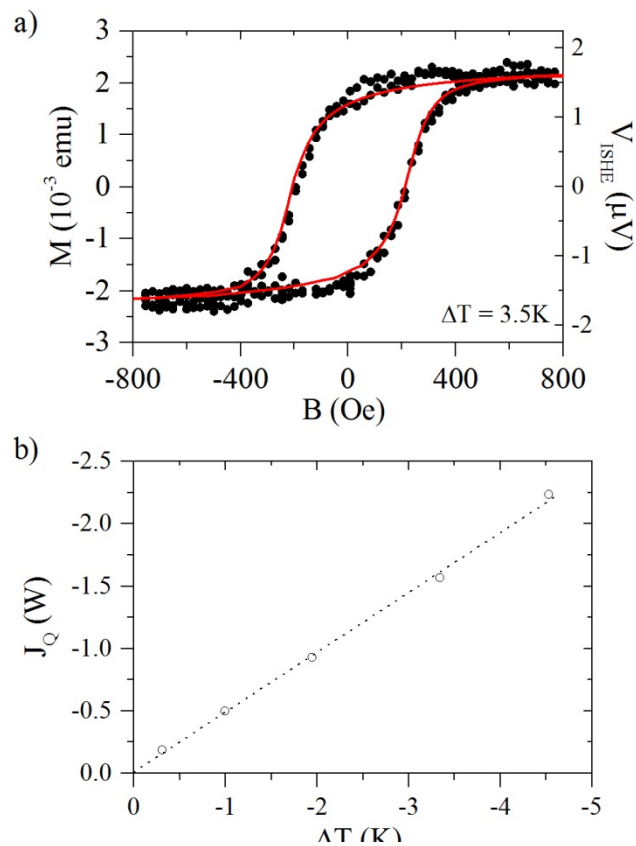


Figure S4 Example spin Seebeck data. a) Raw spin Seebeck voltage, V_{ISHE} , as a function of applied magnetic field plotted alongside corresponding SQUID magnetometry. b) Example variation in temperature difference, ΔT as the heat flux, J_Q , was varied.

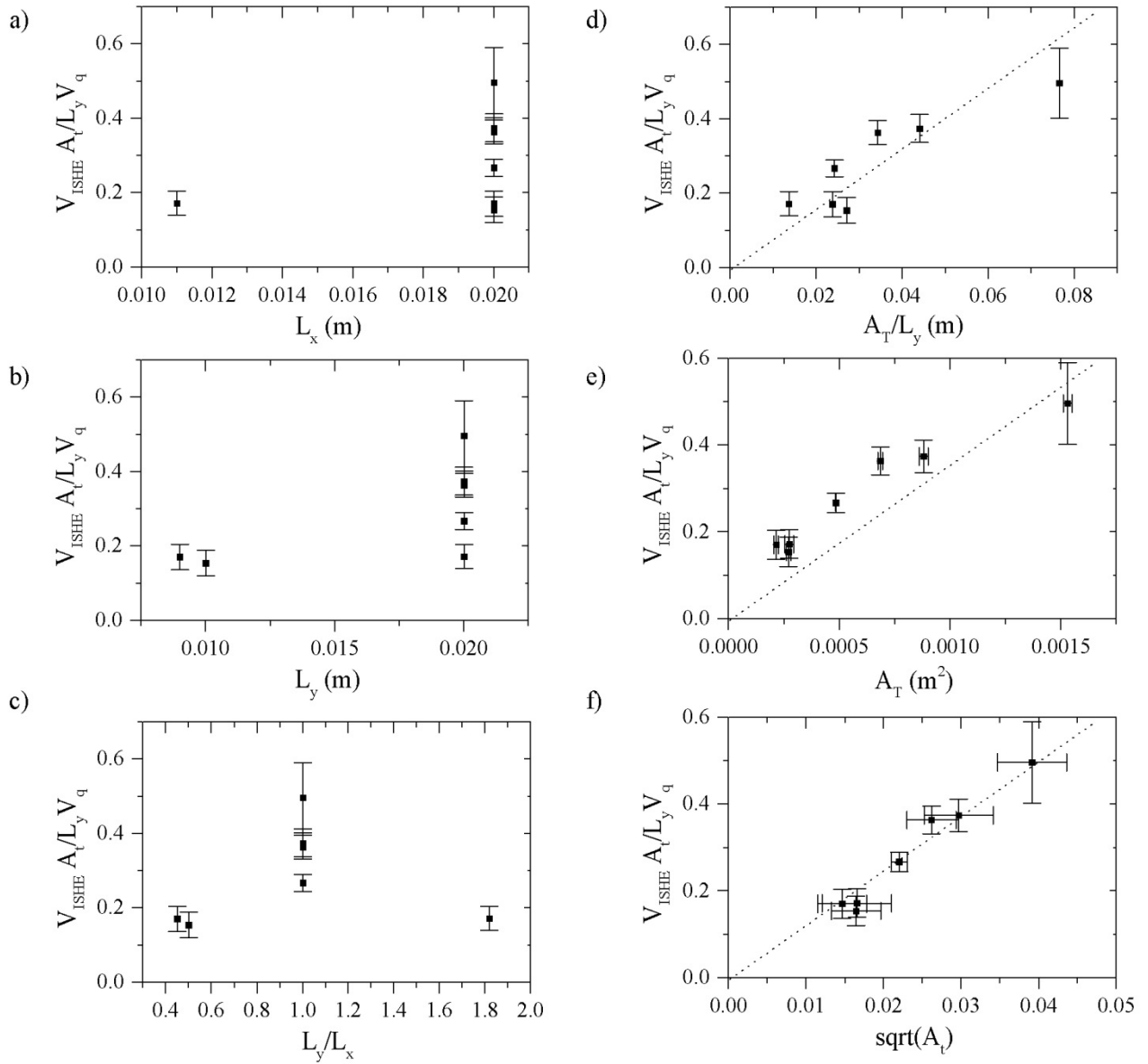


Figure S5 (a) – (f) Spin Seebeck measurement(s) of sample G34 as A_T , L_x and L_y were varied, plotted against L_x , L_y , L_y/L_x , A_T/L_y , A_T and $A_T^{0.5}$.